Corrosion Behavior of MgO-C Ladle Refractory by Molten Slag

Zhao, Qing; Zheng, Xiang; Liu, Chengjun; Jiang, Maofa; Saxén, Henrik; Zevenhoven, Ron

Published in:
Steel Research International

DOI:
10.1002/srin.202000497

Published: 01/04/2021

Document Version
Accepted author manuscript

Document License
Publisher rights policy

Corrosion Behavior of MgO–C Ladle Refractory by Molten Slag

Qing Zhao, Xiang Zheng, Chengjun Liu, Maofa Jiang, Henrik Saxén, Ron Zevenhoven*

Prof. Q. Zhao, Dr. X. Zheng, Prof. C. Liu, Prof. M. Jiang
Key Laboratory for Ecological Metallurgy of Multimetallic Mineral (Ministry of Education), Northeastern University, Shenyang 110819, China
School of Metallurgy, Northeastern University, Shenyang 110819, China
E-mail: srxzx11@163.com

Prof. H. Saxén, Prof. R. Zevenhoven
Process and Systems Engineering Laboratory, Åbo Akademi University, Åbo/Turku 20500, Finland

Keywords: MgO–C refractory, molten, corrosion, refining, $CaO–SiO_2–Al_2O_3–MgO–FeO$ slag

The damage of ladle refractory, which mainly occurs at the position of the slag line, results in an increasing need of maintenance and repair and can in the worst case lead to a break–out of melts causing potential risks for the personnel and damage of equipment. On the basis of this fact, the corrosion behavior of MgO–C refractory in contact with molten slag during the steel refining process was experimentally studied in this work. Rotating and static dipping tests of MgO–C refractory in $CaO–SiO_2–Al_2O_3–MgO–FeO$ slags were conducted, and effects of composition of slag, carbon in refractory and rotation speed on the corrosion behavior were investigated. Results showed that the corrosion depth of the MgO–C refractory increased with FeO content of slag and rotation speed of MgO–C rod, while it decreased with an increase of slag basicity. Slag notably penetrated the surface layer of MgO–C refractory after the carbon was oxidized, causing an aggravation of the corrosion. Moreover, the corrosion mechanism of MgO–C refractory in molten slag during the refining process was studied and illustrated in this work.

1. Introduction

With the rapid development of metallurgical industry with increased throughput, new raw materials and product grades, and higher requirements on the durability of the processing units, the corrosion effect ladle refractory suffers from has become an important issue. The damage

of ladle refractory, which mainly occurs at the position of the slag line, results in an increasing need of maintenance and repair and can in the worst case lead to a break–out of melts causing potential risks for the personnel and damage of equipment. [1] To reduce corrosion, magnesia–carbon (MgO–C) refractories are widely used in the ladle slag line due to their excellent thermal shock, slag, and high–temperature resistance.[2] However, the oxidation of carbon and dissolution of MgO–C refractory into molten slag is still a problem for the refining process.[3, 4] Furthermore, the corrosion products of the refractory often act as a source of harmful inclusions during the refining process of steel, affecting the quality of the steel products.[5–7] Therefore, it is important to understand the corrosion behavior of MgO–C ladle refractory in contact with molten slag during the refining process of steels and the factors that affect the corrosion behavior.

The corrosion effect of different types of metallurgical molten slags on the MgO–C refractory has been studied in earlier investigations, and several mechanisms have been proposed based on specific scenarios. Efendy et al. studied the corrosion mechanism of MgO–C refractory in contact with $CaO–Al_2O_3–SiO_2–MgO$ slag and found that slag penetration and refractory dissolution caused the MgO–C refractory damage.[8] The dissolution of the refractory was found to be the limiting step of the corrosion process of the MgO–C refractory. [9] Huang et al. studied the dissolution behavior of MgO–C refractory in $CaO–Al_2O_3–SiO_2$ slag that was stirred by flowing argon gas at 1773 K.[10] They found that the mass transfer of MgO in the penetrating slag at lower gas flowrates was the rate–controlling step. While Ar bubbles covered the surface and blocked the contact between the liquid slag and the solid phase, reducing the dissolution rate at high gas flowrates. To suppress the dissolution, Luz et al. adjusted and optimized the slag composition as to reduce the corrosion effect.[11] Benavidez et al. and Wang et al. found that the penetration of slag of high basicity occurred at the fine grain boundaries of MgO and segregated MgO grains from the refractory structure.[12,13] Zhang et al. investigated the influence of the basicity of $CaO–MgO–SiO_2$ slag on its penetration into refractory materials.[14]

They claimed MgO refractories to exhibit excellent resistance to slags with a basicity above 1.5 or 2.0. Liu et al. studied the corrosion of MgO–C refractories contacted with $CaO–SiO_2–Al_2O_3–V_2O_5–FeO$ slag and found that slag could penetrate the refractory through the channels formed as the redox reaction of carbon, which led to a refractory degradation.[15] MgO dissolution and chemical reaction between slag and the refractory also altered the wetting and spreading process and increased the rate of refractory corrosion. Han et al. studied the corrosion of MgO–C refractory materials in contact with $SiO_2–Fe_2O_3–V_2O_5–TiO_2–MnO–MgO$ slag through dynamic experiments.[16] They found that carbon was oxidized by oxygen or reducing slag and that dispersed MgO grains were corroded by vanadium–containing slag. Guo et al. studied the corrosion of MgO–C refractory in $CaO–Al_2O_3–SiO_2–MgO–Cr_2O_3$ stainless steel slag with high Al_2O_3 content (~ 15%–wt) using the rotating rod test in a vacuum induction furnace.[17] The results showed that the intrinsic reaction of refractory materials was more crucial than extrinsic decarburization from atmospheric oxygen. Mattila et al. pointed out that converter slag usually contains some FeO, which caused MgO–C refractory wearing.[18] Lu et al. claimed that the oxidation of carbon was the reason for damaged MgO–C refractory.[19]

In summary, although there have been many studies on the corrosion of MgO–C refractory, the corrosion effects of a slag with evolving composition during ladle refining has not been reported.[20] Likewise, the MgO–C refractory decarbonized after first usage has not been reported in the open literature. These are the main motivations behind the present work, which aims at gaining a better understanding of the corrosion behavior of MgO–C refractory during the ladle refining process. The influence of slag compositions and rotation speed on the corrosion behavior of MgO–C refractory immersed in a $CaO–SiO_2–Al_2O_3–MgO–FeO$ slag was investigated by rotating and static dipping cylindrical refractory specimens in a crucible. The findings of the study can be useful in the design of improved processing conditions and refractory materials.

2. Experimental

2.1. Material

Final compositions of converter slag and refining slag in a steel plant were analyzed and are reported in **Table 1**. Based on compositions of these slags, considering the evolution of slag compositions in the ladle furnace (LF) refining process, experimental slags with different basicity (defined as the mass ratio $B = CaO/SiO_2$) and FeO content were designed and produced, named M1–M4 (cf. **Table 2**). The basicity of these are in the range $B = 2.5 \sim 3.5$ and the FeO contents vary from 1%–wt to 15%–wt. The samples were prepared by mixing chemical reagents calcium oxide ($CaO \geq 98.0\%$–wt), silicon oxide ($SiO_2 \geq 99.0\%$–wt), magnesium oxide ($MgO \geq 99.9\%$–wt), aluminum oxide ($Al_2O_3 \geq 99.0\%$–wt), and ferrous oxalate ($FeC_2O_4 \cdot 2H_2O \geq 99.9\%$–wt). All reagents were purchased from Sinopharm Chemical Reagent Co., Ltd., China, and were dried at 110 °C for 10 h before weighing and mixing.

MgO–C rods (diameter 13 mm, length 50 mm) were cut from a commercial brick used for the same steel plant. Chemical compositions, density, porosity, and crushing strength of the MgO–C refractory used in this study are listed in **Table 3**. The density and porosity of refractory were measured by Archimedes method. To investigate the corrosion behavior of the MgO–C refractory serving for a period (i.e., carbon in the surface layer has been consumed), a MgO–C sample was pre–decarburized at 1000 °C for 15 min in the muffle furnace before corrosion experiments.

2.2. Method

Figure 1 illustrates the furnace used for rotating and static dipping tests of MgO–C refractory. The furnace is equipped with the $MoSi_2$ as heating elements (5KW per element), and two B–type thermocouples were used to measure and for control of the temperature. The temperature–control accuracy of the system is ± 1 °C. The graphite crucible (inner diameter 40 mm, outer diameter 48 mm, height 70 mm) containing 150 g of the synthetic slag, was placed in the furnace at room temperature and heated to the target temperature in argon (purity 99.99%–wt)

atmosphere and held for 30 min at that temperature to achieve a fully molten state. The MgO–C refractory specimen was then immersed into the molten slag and rotated at different speeds (0 ~ 180 rpm) for 45 minutes. Finally, the refractory specimen was taken out and slowly cooled to room temperature.

Test parameters, such as temperature, immersion time and rotation speed, are reported in **Table 4**. The rotation speed of the refractory sample was varied in the range from 0 rpm (i.e. static state) to 180 rpm to investigate the effect of the mass transfer rate of the slag phase on the corrosion rate. The immersion time was set to 45 minutes. The viscosity and activity values of the experimental slags at 1550 ℃ were calculated by FactSage 8.0 software (CTT–Technology, Aachen, Germany) and reported in **Table 5**.

After the experiments, the samples were polished and gold–sprayed to give conductivity for scanning electric microscope–energy dispersive spectroscopy (SEM–EDS) analysis. SEM–EDS analysis was conducted using a Phenom pro X device (Eindhoven, The Netherlands) to investigate the micromorphology and chemical composition of the MgO–C refractory after corrosion. The refractory specimens were cut in the diameter direction at the point of maximum radius change, and the cross–sectional topography was obtained via SEM analysis. The cross–sectional area was determined by the Image Pro plus 6.0 software and the radius of the refractory material is expressed as an equivalent circle radius. The corrosion depth (Δr) was used to estimate the degree of corrosion, which defined by

$$\Delta r = r - \sqrt{\frac{S}{\pi}} \tag{1}$$

where r is the initial radius of the rod and S is the cross–sectional area of the rod after corrosion test.

3. Results and Discussion

3.1 Effect of FeO content

SEM images of the corrosion interface between the slag with different FeO contents (15%–wt, 5%–wt and 1%–wt) and the MgO–C refractory specimens are shown in **Figure 2**. The EDS

results of the phases in Figure 2(a) are listed in **Table 6**. As can be seen from Figure 2, a new metallic iron phase (bright white) generated in the interface layer. The size of iron phase is over than 300 μm after the MgO–C refractory reacted with high FeO molten (15%–wt) and is less than 100 μm when the slag contains low FeO content (5%–wt). Only a slight amount of metallic iron was formed in the slag when the FeO content was low (1%–wt). The changes of standard Gibbs free energy of the reactions between carbon and CaO, SiO_2, Al_2O_3, MgO, and FeO were calculated by Inorganic Thermodynamic Data Manual, respectively.[21] According the activity of the slag listed in Table 5, a $\Delta G \sim P_{CO}/P^{\theta}$ diagram of chemical reactions between C and components in M1 slag was plotted and is shown in **Figure 3**. Results showed that the Gibbs free energy of the reaction of C with (FeO) at 1550°C is more negative than the other reactions at different P_{CO}/P^{θ}. Therefore, the consumption of carbon of MgO–C refractory mainly caused by the FeO reduction. The large–sized iron phase observed in the interface layer may be formed through a metallic iron aggregation due to the difference in interface tension between iron and slag. From Figure 2(a), it was found that when the slag was rich in FeO (15%–wt), a FeO ring formed and covers on the surface of the iron phase, which is attributed to the iron oxidation by oxygen and molten slag. Similar results have been reported by other investigators.[22] A (Mg, Fe)O phase was reported by researchers while was not found in this study.[23] This could be due to the severe reduction reaction between the C and FeO, generating a Fe as a product (cf. Figure 2).

Figure 4 illustrates the effect of FeO content on the corrosion depth of the MgO–C refractory. As can be seen from Figure 4 that the corrosion depth decreases with a decrease in FeO content. Carbon in the MgO–C refractory can depress the wettability between the refractory and the slag.[24, 25] Therefore, the large consumption of carbon in refractory could lead to the slag penetrated the refractory more easily. Moreover, several studies indicated that the viscosity of molten is of vital importance to the penetration behavior and changed during the smelting process, which is significant to help to understand the internal relationship between the

chemical composition, physical property and corrosion ability of the molten slag.[26,27] The viscosity decreases with the FeO content, meaning the physical erosion of molten slag to the refractory is more seriously when the FeO content of slag is high.

3.2 Effect of Carbon

In view that MgO–C refractory at the slag line is always decarbonized after a period of serving time. A decarburized MgO–C refractory was prepared before the corrosion experiment (MgO–C refractory pre–treatment) as to simulate the corrosion behavior of the refractory after first usage. SEM images and EDS results of the pre–treated and untreated MgO–C refractory after contact with molten M1 at 1550 °C for 45 min presented in **Figure 5**(a) and (b), respectively. As can be seen from Figure 5(a), the slag significantly penetrates the pre–treated MgO–C refractory and wraps the MgO particle in a thick layer. The slag permeated the MgO–C refractory along the MgO grain boundaries and the channels which formed as the decarburization process before the sample was immersed into the slag melt, resulting in dissociation of the MgO aggregate. In contrast, the thickness of the slag layer on the surface of the MgO particle in refractory sample without pre–treatment was thin (cf. Figure 5(b)) due to the anti–wetting effect of graphite on molten slag.[24,25] Microscopic analysis showed that the corrosion depth of the refractory untreated specimen in contact with M1 slag was about 0.28 mm, whereas the corrosion depth for the pre–treatment specimen was about 1.70 mm.

3.3 Effect of basicity

Refining slags of different basicities are used in the production of different steel grades. The slags also absorb inclusions during the refining process, resulting in a change of slag basicity. **Figure 6** shows SEM images and EDS results of the interface between the molten slag of different basicities (B = 3.5 and 3.0) and the MgO–C refractory specimens. It can be seen that the interface between the refractory and slag was clearly visible when the slag basicity was 3.5, and the extent of corrosion of MgO aggregates was more serious when B = 3.0. No significant change in corrosion morphology of specimens can be observed when the basicity became lower

(B = 2.5) in this study. Figure 6(b) shows that the slag penetrated the MgO aggregates through the grain boundaries and corroded them, causing some small MgO particles released from the refractory to the molten slag. Multi–component phase diagram of the CaO–SiO_2–MgO–35% Al_2O_3 system in the slag atlas indicates that the composition of M4 is near the saturation line of melilite,[28] and the composition of M2 is near the saturation line of the periclase, meaning M4 possesses a stronger dissolving capacity to the MgO phase in the refining process.[29] And as the basicity decreases from 3.5 to 3.0, the liquidus line of 1550℃ expands in the direction of increasing MgO content. This explains why the extent of corrosion of MgO–C refractory was more severe by low–basicity slags.

Figure 7 outlines a possible dissolution process of MgO–C refractory in molten slag. MgO in the refractory readily reacts with Ca, Si, and Al oxides to form low–melting phases (such as melilite) and be melted into the slag phase. Therefore, some oxides in the bulk molten diffuse to the surface of refractory and corrode the MgO aggregates of MgO–C refractory. Grain boundaries and the channels formed as the carbon consumption could provide the paths for molten penetrating.[30] Particles of MgO peeled from the matrix of refractory disperse into the molten leading to a decrease of radius of rod from the r_0 to r_t. Some of the particles may not be able to dissolve in the molten during the refining process if the MgO in slag reaches the saturation state.

3.4 Effect of scour of molten slag

The surface of working layer of refractory are subjected to scouring attack of melt and molten slag during the refining process. MgO saturation of slags at can be estimated in the temperature range 1500 ~1620 °C by [31]

$$(\%\mathrm{MgO})_s = 8.2/R + 0.06(\%\mathrm{FeO}) + 0.2(\%\mathrm{CaF_2}) + 0.019(T - 1550) \quad (2)$$

for slags with a ternary slag basicity

$$R = \%\mathrm{CaO}/(\%\mathrm{Al_2O_3} + \%\mathrm{SiO_2}) \quad (3)$$

falling in the range of R = 0.7 ~ 1.5.

This equation shows that MgO in M1 had reached a saturated state at 1550 °C, and it is therefore difficult for MgO in the refractory to dissolve. The maximum rotation speed studied in this work was determined by surface velocity of melt (v_s). The critical Weber number of slag entrapment is 6.039, in which of the situations the v_s is about 0.42 m/s.[32] The relationship between the rotation speed (n) and v_s is given by the expression

$$\frac{n}{60} \cdot 2\pi r = v_s \tag{4}$$

Therefore, the maximum rotation speed was determined to 180 rpm.

Figure 8, which shows the corrosion depth of MgO–C refractory in molten M1 with different rotation speeds at 1550°C, clearly demonstrates that the corrosion depth increased with the rotation speed. As can be seen in Figure 8 that, after the refractory immersed into the static molten M1 for 45 min, the corrosion depth was about 0.28 mm. As for the refractory rod rotated in the molten M1 at a speed of 90 rpm, the corrosion depth reached about 0.42 mm. Moreover, the corrosion depth went to about 0.52 mm when the rotation speed increased to 180 rpm. The shear stress generated at the interface between the specimen and the molten slag peels off the MgO aggregates near the interface, and this effect is stronger at higher rotation speed.

SEM images of the MgO–C refractory/slag interface after immersion in molten M1 are presented in **Figure 9**. As can been seen from Figure 9, the slag penetrated at the grain boundary of MgO aggregates. Similar phenomena have been reported by other investigators.[30] It is noteworthy that, unlike the calculated corrosion depth, the difference in infiltration depth is non–significant in the SEM images. A reason for this is/may be that the slag penetrated the refractory, and the refractory containing slag peeled from the MgO–C refractory under the high rotation speed. Slag penetration into the refractory occurs rapidly by slag infiltration through pores and cracks, but penetration is slow by slag infiltration through grain boundaries.

4. Conclusion

The corrosion behavior of MgO–C refractory was investigated in experiments where cylindrical refractory specimens were rotated or dipped in $CaO–SiO_2–MgO–Al_2O_3–FeO$ slag in a crucible. The corrosion behavior of the refractory after first usage was simulated. The results indicated that the depth of corrosion in the MgO–C refractory increased with rotation speed, while it decreased with an increase of slag basicity. Carbon in refractory oxidized by FeO when the refractory with FeO–rich slag, and the degree of corrosion of the refractory increased with the FeO content. Due to the oxidation of carbon in the MgO–C refractory, the wettability between the refractory and the molten slag decreased, which led to a penetration of slag and aggravated the corrosion.

Conflict of Interest: The authors declare no conflict of interest.

Acknowledgements

The authors gratefully acknowledge supports by the National Key R&D Program of China [2017YFC0805100], the National Natural Science Foundation of China [No. 51704068], the Liaoning Provincial Natural Science Foundation of China [No. 2019–MS–127], and the Fundamental Research Funds for the Central Universities [No. N2025035 and N180725008].

Received: ((will be filled in by the editorial staff))
Revised: ((will be filled in by the editorial staff))
Published online: ((will be filled in by the editorial staff))

References

[1] S. Song , J. Zhao , P. C. Pistorius, *Metall. Mater. Trans. B*. **2020**, *51*, 891.

[2] T. Zhu, Y. Li, S. Sang, *J. Alloy. Compd*. **2019**, *783*, 990.

[3] S. Akkurt, H.D. Leigh, *Am. Ceram. Soc. Bull*. **2003**, *82*, 32.

[4] S. Jansson, V. Brabie, P. Jönsson, *Scand. J. Metall.* **2005**, *34*, 283.

[5] S. Jansson, *Degree Thesis*, Royal Institute of Technology, Stockholm, May, **2005**.

[6] M. Chen, S. Gao, L. Xu, N. Wang, *Ceram. Int*. **2019**, *45*, 21023.

[7] S. Akkurt, *Degree Thesis*, Clemson University, South Carolina, August, **1998**.

[8] H. Efendy, M. Safarudin, H. Sihombing, *Int. J. Eng. Tech.* **2010**, *10*, 40.

[9] M. Lee, S. Sun, S. Wright, S. Jahanshahi, *Metall. Mater. Trans. B.* **2001**, *32*, 25.

[10] F. Huang, C. Liu, N. Maruoka, *Ironmak. Steelmak*. **2015**, *42*, 553.

[11] A. P. Luz, F. C. Leite, M. A. M. Brito, V. C. Pandolfelli, *Ceram. Int.* **2013**, *39*, 7507.

[12] E. Benavidez, E. Brandaleze, L. Musante, P. Galliano, *Procedia Materials Science.* **2015**, *8*, 228.

[13] W. Wang, L. Xue, T. Zhang, L. Zhou, J. Chen, Z. Pan, *Ceram. Int.* **2019**, *45*, 20664.

[14] W. Zhang, A. Huang, Y. Zou, H. Gu, L. Fu, G. Li, *J. Am. Ceram. Soc.* **2020**, *103*, 2128.

[15] Z. Liu, L. Yuan, E. Jin, X. Yan., J. Yu, *Ceram. Int*. **2019**, *45*, 718.

[16] B. Han, C. Ke, Y. Wei, W. Yan, C. Wang, F Chen, N. Li, *Ceram. Int*. **2015**, *41*, 10966.

[17] M. Guo, P.T. Jones, S. Parada, E. Boydens, J.V. Dyck, B. Blanpain, P. Wollants, *J. Eur. Ceram. Soc.* **2006**, *26*, 3831.

[18] R.A. Mattila, J.P. Vatanen, J.J. Härkki, Scand. *J. Metall.* **2010**, *31*, 241.

[19] C. Lu, X. Lu, X. Zou, H. Cheng, G. Li, Y. Bian, X. Xie, K. Zheng, The 6th International Symposium on High–Temperature Metallurgical Processing, Orlando, Florida, **2015**.

[20] Y. Li, W. Yang, L. Zhang, *Metals*. **2020**, *10*, 444.

[21] Y. Liang, Y. Che, *Inorganic Thermodynamic Data Manual*, Northeastern University Press, Shenyang, China **1993**.

[22] P. Shen, L. Zhang, Y. Wang, W. Yang, *Steelmaking*. **2016**, *32*, 54.

[23] M. K. Cho, M. V. Ende, T. H. Eun, I. H. Jung, *J. Eur. Ceram. Soc*. **2012**, *32*, 1503.

[24] Z. Liu, J. Yu, X. Yang, *Materials*. **2018**, *11*, 883.

[25] A.S. Mehta, V. Sahajwalla, *Scand. J. metal*. **2000**, *29*, 17.

[26] J. H. Park, M.O. Suk, I. H. Jung, M. Guo, B. Blanpain, *Steel Res. int.* **2010**, *81*, 860.

[27] J. S. Han, J. G. Kang, J. H. Shin, Y. Chung, J. H. Park, *Ceram. Int*. **2018**, *44*, 13197.

[28] L. Chen, A. Malfliet, P.T. Jones, B. Blanpain, M. Guo, *Metall. Mater. Trans. B.* **2019**, *50*, 1822.

[29] J. Han, J. Heo, J. Park, *Ceram. Int*. **2019**, *45*, 10481.

[30] M. Guo, S. Parada, P.T. Jones, E. Boydens, J.V. Dyck, B. Blanpain, P. Wollants, *J. Eur. Ceram. Soc*. **2009**, *29*, 1053.

[31] L. Sun, J. Li, R. Zhang, T. Huang, L. Wang, *Industrial Heating*. **2013**, *42*, 45.

[32] S. Riaz, K.C. Mills, K. Bain, *Ironmak. Steelmak.* **2013**, *29*, 107.

Figures and Tables

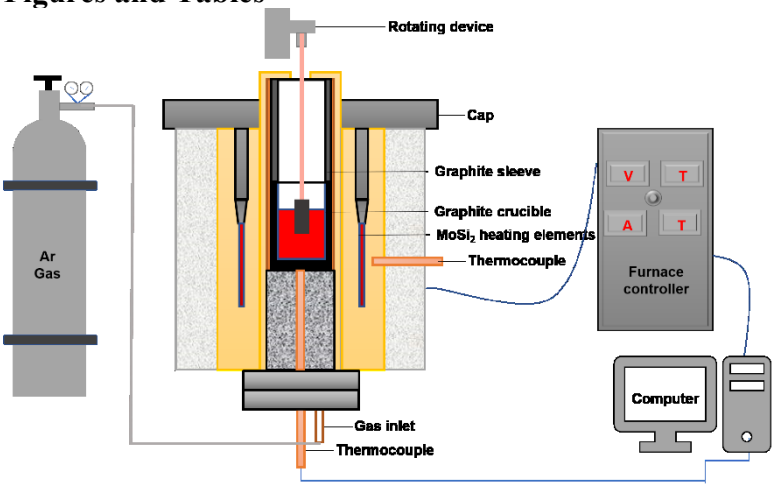

Figure 1. Illustration of the furnace used in the study.

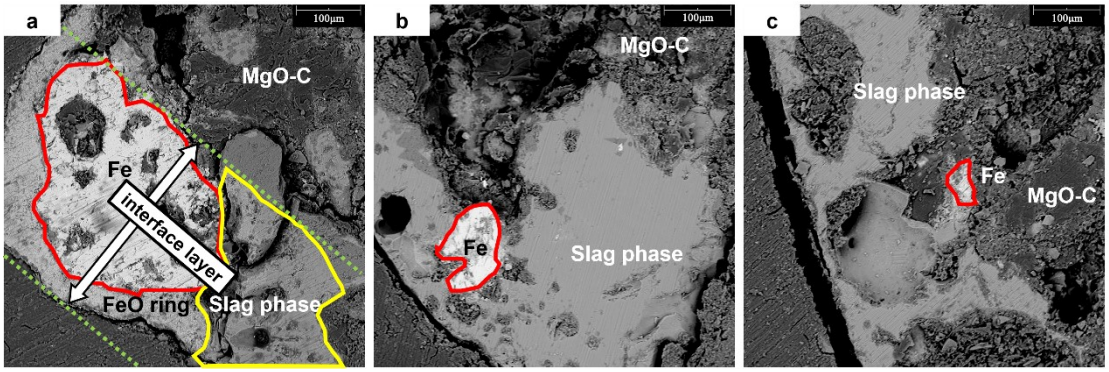

Figure 2. SEM images of the corrosion interface between the slag with different FeO contents and the MgO–C refractory specimens, (a) 15%–wt FeO, (b) 5%–wt FeO, (c)1%–wt FeO.

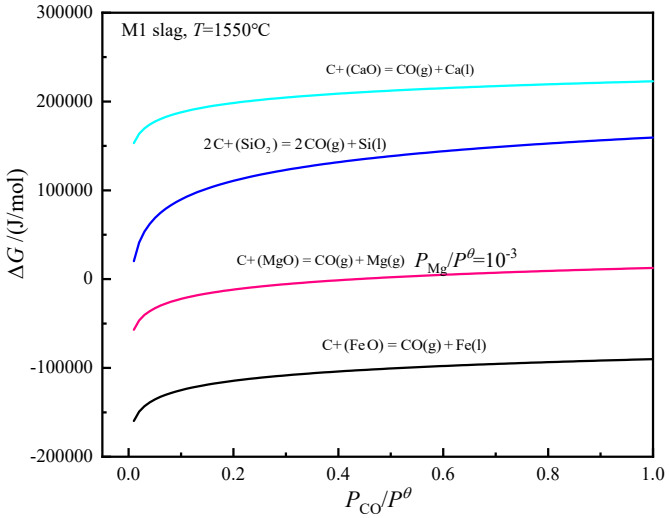

Figure 3. $\Delta G \sim P_{CO}/P^{\theta}$ diagram of chemcial reactions between C and components in M1 slag.

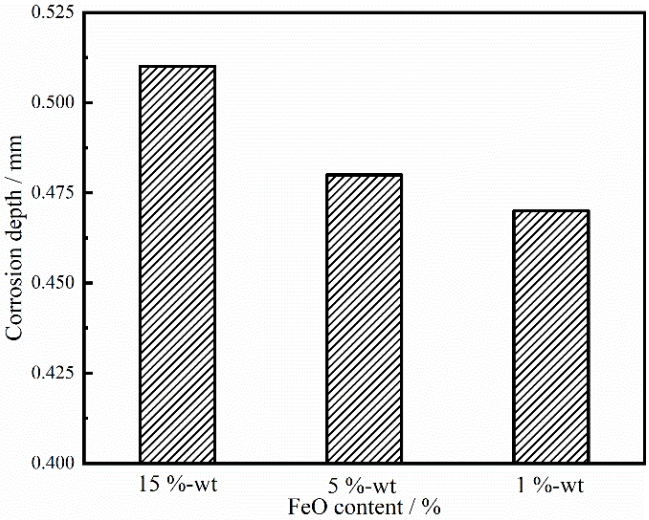

Figure 4. Effect of slag FeO content on the corrosion depth of MgO–C refractory (1550 °C, 180 rpm).

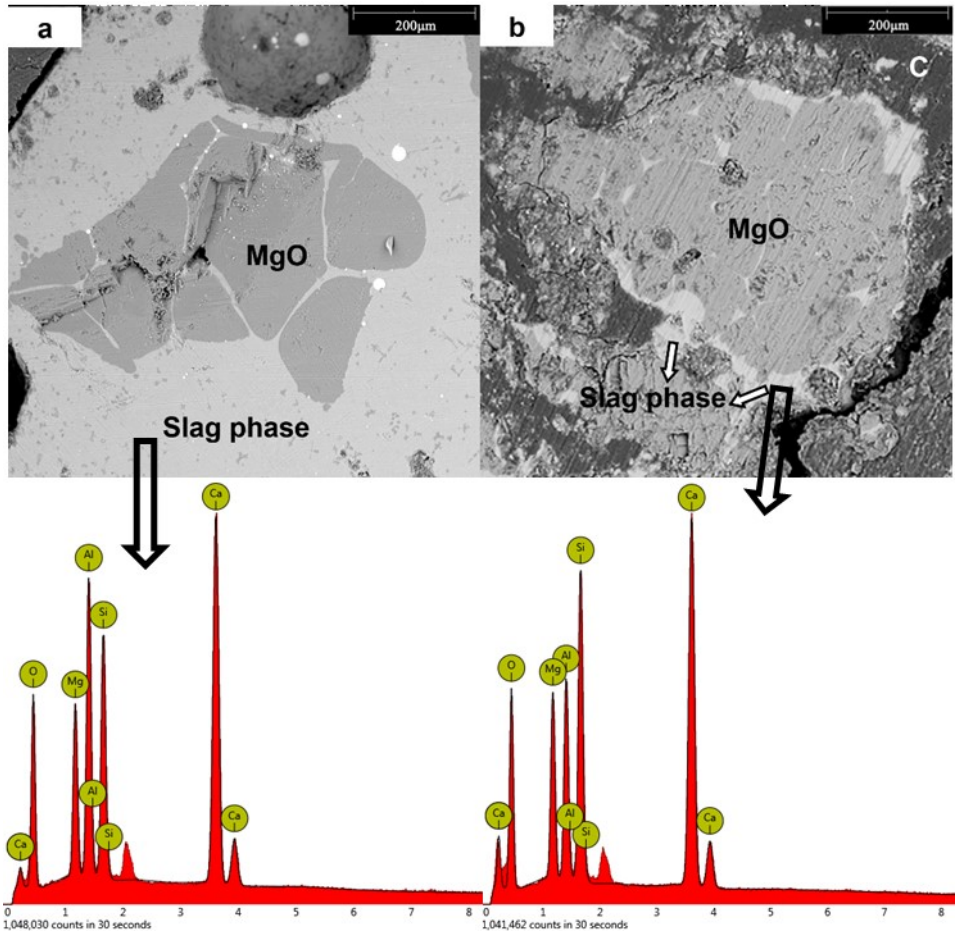

Figure 5. SEM images and EDS results of (a) pre–treated and (b) untreated MgO–C refractory samples after contact with molten M1 at 1550 °C for 45 min.

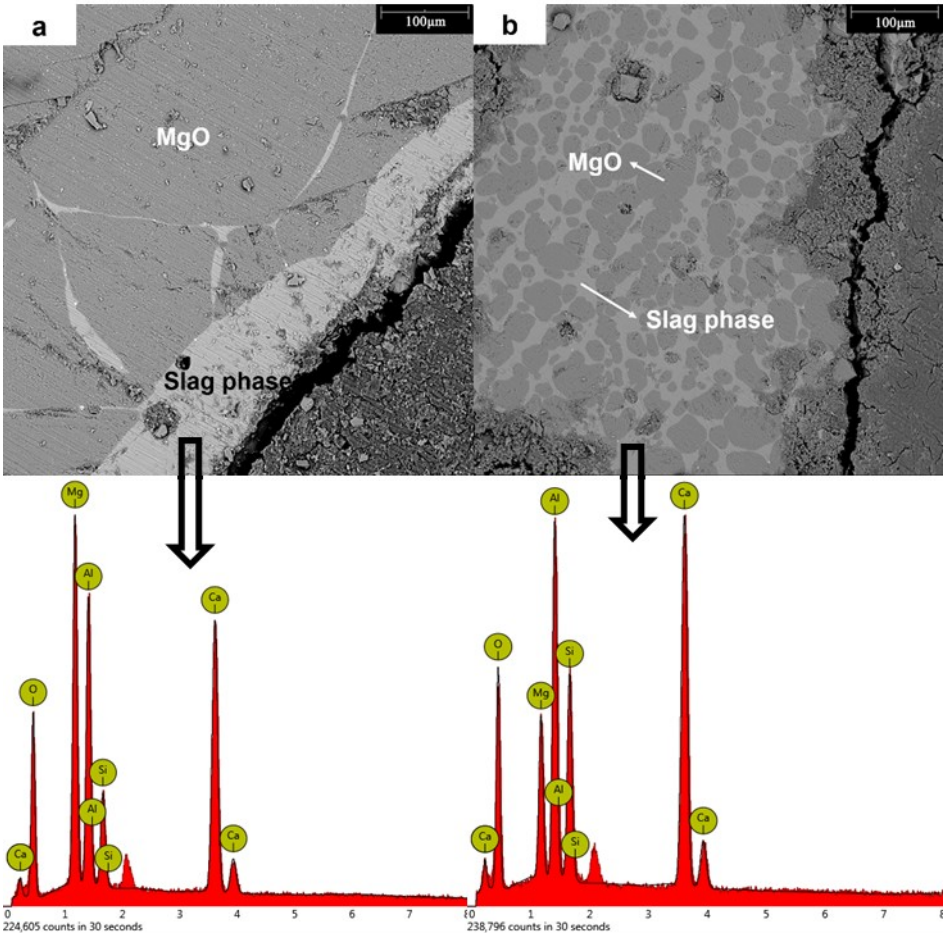

Figure 6. SEM images and EDS results of the interface between the molten slag of different basicities, (a) B = 3.5 and (b) 3.0, and the MgO–C refractory specimens.

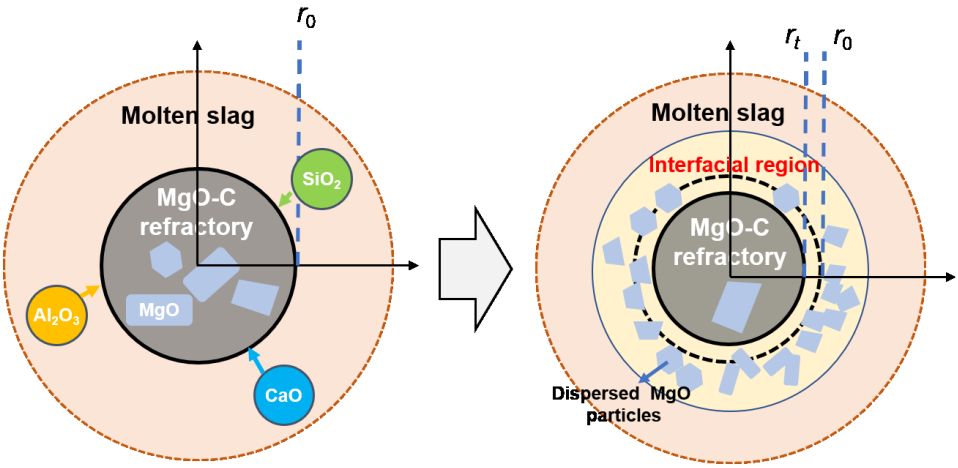

Figure 7. Corrosion mechanism of MgO–C refractory in molten slag.

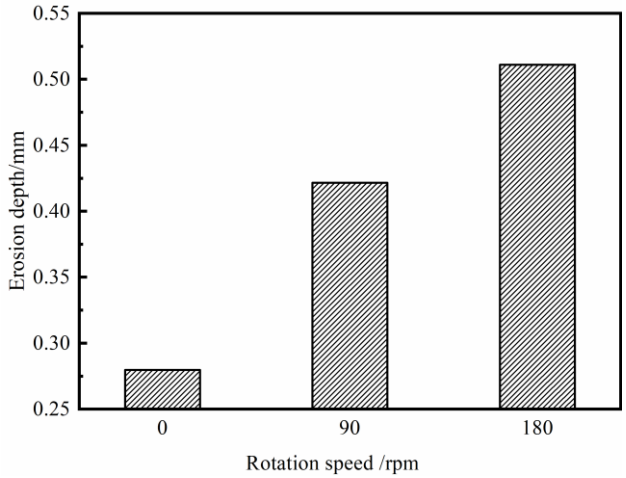

Figure 8. Effect of rotation speed on the corrosion depth of MgO–C refractory.

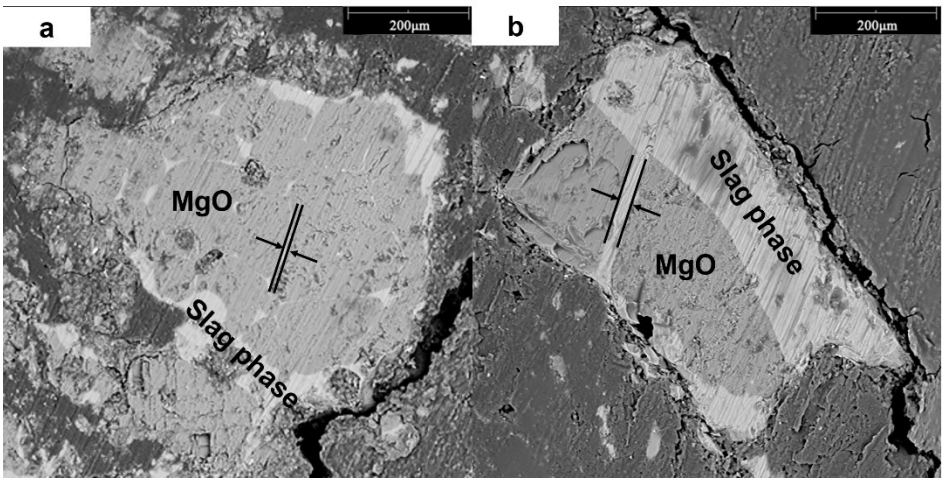

Figure 9. SEM images of MgO–C refractory/slag interface after immersion in M1 slag at 1550 °C with the rotation speeds of (a) 0 rpm, (b) 180 rpm.

Table 1. Final compositions of converter slag and refining slag (mass fraction [%], dry).

Items	CaO	SiO_2	FeO	MgO	Al_2O_3
Converter final slag	40.3	16.3	15.0	9.1	19.3
Refining slag 1	45.3	12.5	1.2	8.7	32.3
Refining slag 2	41.1	11.9	5.7	9.0	32.3

Table 2. Chemical compositions of experimental slags (mass fraction [%], dry).

Exp. Set.	CaO	SiO_2	FeO	MgO	Al_2O_3	*B*
M1	40	16	15	9	20	2.5
M2	41	12	1	9	37	3.5
M3	38	13	5	9	35	3.0
M4	40	13	1	9	37	3.0

Table 3. Chemical compositions, density, porosity, and crushing strength of the MgO–C refractory used in this study (dry).

MgO [%]	C [%]	Others [%]	Density [$kg \cdot m^{-3}$]	Porosity [%]	Crushing strength [Mpa]
78.0	14.0	8.0	2950	8.0	40.0

Table 4. Parameters for the experiments.

Exp. Set.	Rotation speed [rpm]	Temperature [°C]	Immersion time [min]
M1, M2, M3, M4	180	1550	45
M1	0, 90, 180	1550	45

Table 5. Slag viscosity and activity of different experimental slag calculated by FactSage 8.0.

Exp. Set.	a(CaO)	a(SiO_2)	a(FeO)	a(MgO)	a(Al_2O_3)	Temperature [°C]	viscosity [Pa·s]
M1	0.034	5.34×10^{-4}	0.229	0.131	6.35×10^{-3}	1550	0.0754
M2	0.036	5.71×10^{-4}	0.002	0.110	1.17×10^{-2}	1550	0.1667
M3	0.027	7.94×10^{-4}	0.011	0.100	1.52×10^{-2}	1550	0.1492
M4	0.031	7.31×10^{-4}	0.023	0.103	1.40×10^{-2}	1550	0.1758

Table 6. Atomic percentages of different regions in Figure 2(a) (molar fraction [%]).

Possible phases	Ca	Si	Fe	Mg	Al	O
Fe	-	-	100	-	-	-
FeO ring	-	-	52.11	-	-	47.89
Slag phase	14.66	12.40	-	7.38	13.19	52.37